Dynamics of He Double Ionisation in the Non Perturbative Regime: The Reduction to an Effective Three-Particle Problem

A. N. Perumal,[1] R. Moshammer,[1] M. Schulz,[2] and J. Ullrich[1]

[1]Max-Planck-Institut für Kernphysik, Saupfercheckweg 1, D-69117 Heidelberg, Germany

[2]University of Missouri-Rolla, Rolla, Missouri 65401

E-mail: Joachim.Ullrich@mpi-hd.mpg.de

Abstract

Double ionisation of He by 3.6 MeV/u Au^{53+} impact is investigated in a kinematically complete experiment using an integrated multi-electron recoil-ion momentum spectrometer (reaction microscope). Surprisingly, the final-state correlation between the recoiling He^{2+} target ion momentum and the momenta of both emitted electrons is found to be the strongest among the various two-body correlations. On this basis it is demonstrated that the four-body momentum balance can be reduced to a good approximation to an effective three-particle problem by considering the centre-of-mass motion of the two electrons instead of their individual momenta. Then, all essential dynamical features observed for single ionisation earlier, like for example a strong forward-backward asymmetry in the longitudinal momentum balance resulting from the final-state interaction with the projectile, are naturally rediscovered. Moreover, important conclusions on the properties of the TS-2 double ionisation mechanism are drawn.

PACS numbers: 34.10+x, 34.50.Fa

1. Introduction

Understanding the dynamics of many-body processes is the subject of increasing research activity in atomic collision physics. As our understanding of single ionisation is rapidly improving (for the case of single ionization of hydrogen by electron impact even a complete solution has been claimed by Rescigno et al. (1999)) research efforts now shift towards double ionisation. Such processes are particularly difficult to describe because one is faced with two major challenges simultaneously: i) the collision dynamics involving a two-centre potential and ii) the interaction between the two active electrons that can lead to pronounced correlation effects. Tremendous experimental as well as theoretical advancements have been achieved during recent years for double photoionisation (γ, 2e) [for a review see Briggs and Schmidt (2000)] and electron impact double ionisation (e, 3e) [see e.g. Taouil et al. (1998); Lahmam-Bennani et al. (1999,2001); Dorn et al. (1999, 2001)]. Double ionisation as a result of ion impact, however, has sparsely been explored particularly in the regime of strong perturbation (defined as the ratio between projectile charge (q) and its velocity (v_p)). Large perturbation collisions are of current attention not only because of their fundamental importance but also because of potential applications in inertial fusion, material science and cancer therapy.

Theoretically, the regime of large perturbation is substantially more challenging, since the highly charged ion interacts simultaneously with two active electrons in the target in addition to the interaction between them and other fragments. Hence, theoretical first order treatments of the projectile-target interaction cannot be applied as for photon or fast charged particle impact and the full problem of mutually interacting four particles (projectile, residual ion and two electrons) has to be solved numerically since there is no closed form analytic solution. Despite this intricacy, several theories have come up in recent years [McGuire et al. (1995) and references therein], but unfortunately those are restricted mainly to the calculation of total cross sections yielding only very limited information about the details of double ionisation. For instance, sophisticated theories like the Forced Impulse Approximation [Bronk et al. (1998)] and the continuum-distorted-wave – eikonal-initial-state (CDW-EIS) [Fainstain et al. (1998)] methods do not yet provide in-depth information such as partial, or fully differential cross sections, the momentum distribution as well as the angular scattering of the fragments. A very recent calculation within this CDW-EIS approach determined the double differential electron emission cross sections for single and multiple ionisations based on an

independent electron treatment [Kirchner et al (2001)]. The classical trajectory Monte Carlo (CTMC) method, in contrast, provides detailed information in momentum space [Wood et al. (1997)], which is often in amazing overall agreement with experiment, but due to the intrinsic limitations, a classical model will not be able to describe the facets of many-particle quantum systems. On the whole, the basic difficulty of theoretical methods forces us to realize the crucial importance to perform detailed experimental investigations in order to explore the underlying dynamic mechanisms responsible for double ionisation, and to advance our understanding of fundamental few-particle quantum systems under the action of a time-dependent force.

At the experimental front on the other hand, kinematically complete measurements (kinematically complete means that the momenta of all collision fragments in the final state but not the spin are determined) on double ionisation display a rapid achievement in recent years. Since the pioneering work of Schwarzkopf et al. (1993), double photoionisation experiments exhibit a considerable progress and a wealth of fully resolved differential cross sections are now available [see e.g. Dörner et al. (1996, 1998), Huetz et al. (2000), Reddish et al.(1997)]. Nearly in parallel with photon impact, electron impact experiments also emerged with detailed double ionisation cross section data by the rigorous experiments of Taouil et al. (1998) and Dorn et al. (1999). Thereby different reaction mechanisms are investigated in detail and the relation to photo double ionisation has been explored for small momentum transfer (Dorn et al. (2001)). Contrary to photon and electron impact studies, ion-impact double ionisation measurements undergo greater difficulties in its progress although it has more flexibility in investigating different perturbation regimes (the charge state and the velocity of the projectile can be chosen accordingly to get a required perturbation strength). The lack of such experiments is mainly due to the limited resolution in directly accessing the momentum change of the projectile, which is usually much smaller than the momentum spread of the ion beam, and the immense difficulties in detecting two low-energy electrons by conventional electron spectroscopy techniques.

These problems have recently been overcome by the advent of multi-electron recoil-ion momentum spectrometers (reaction microscopes) based on ultra-cold supersonic jet targets and an efficient detection of two low-energy electrons along with the recoiling target ion. This technique offers benchmark studies for theories and provides significant insight into collision mechanisms responsible for the ionisation process. For instance, the first and foremost

kinematically complete experiment on double ionisation of helium by Se^{28+} impact was reported by Moshammer et al. (1996) for a perturbation strength q/v_p of 2.2 (in atomic units, i.e., $m_e = \hbar = 1$), where the longitudinal momentum distributions are discussed. This was followed by a detailed measurement by Bapat et al. (1999,2000), where electron angular distributions and the role of momentum transfer as well as of correlated initial states were analysed for double ionisation of helium by 100 MeV/u C^{6+} impact at a small perturbation of about 0.1. Schulz et al. (2000) developed a new method to study electron-electron correlation effects in double ionization independently of the collision dynamics using the correlation function. Evidence for viewing ground state electron correlation was reported recently (Mergel et al. (2001)) in proton on helium transfer ionisation experiments.

Kinematically complete measurements for heavy-ion impact double ionisation of helium in the large perturbation regime, describing the momentum balance both in longitudinal (the direction along the projectile motion) and transverse directions (perpendicular to the projectile motion) as well as the angular scattering of collision fragments have not been reported in detail until now. Moreover, comparisons between double ionisation and single ionisation were only made for small perturbation (Giese et al (1988)), although it seems to be quite reasonable to put forward such a comparison in the large perturbation regime where double ionisation is acknowledged as two independent single ionisation like events. This can be easily visualized by comparing the centre-of-mass motion of two electrons in double ionisation with the motion of one electron in single ionisation; thereby we can disclose the similarities between these two different ionization processes.

Keeping these aspects in mind, we have done a kinematically complete measurement for large perturbation ($q/v_p = 4.4$) and explored the momentum balances of the fragments in detail. Several projections of the “effective” three-particle momentum space on to the collision as well as the azimuthal plane are reported here in order to investigate whether such a reduction of the four particle problem is reasonable and thus reveals further insight into the double ionisation process (note that the centre of mass motion of two electrons is taken as the motion of one effective particle, disregarding any electron-electron correlation). The angular correlation between the three effective collision fragments is investigated in detail, and selected single differential cross sections are presented. Signatures of the electron-electron correlation have been reported previously and further will be explored in a subsequent publication.

2. Experiment

The experiments were performed using a well collimated (1 x 1 mm^2) and charge-state analysed 3.6 MeV/u Au^{53+} beam from the UNILAC accelerator at GSI. The technical detail of the reaction microscope is found in Moshammer et al. (1996), therefore, only a brief description is provided here. The ion beam is crossed with a well-defined helium target from a two-stage internally cold supersonic gas jet. Recoiling target ions and both electrons produced in the reaction zone are extracted along the ion beam into opposite directions by a weak uniform electric field of about 1.3 V/cm applied on two parallel resistive plates over a length of 22 cm. An additional homogeneous magnetic field of 10-20 Gauss, generated by two Helmholtz coils (1.5 m diameter), is applied almost parallel to the electric field vector forcing the electrons on cyclotron trajectories with a radius proportional to their transverse momentum component. This ensures that all electrons with transverse momenta of less than ~ 3.5 a.u. are recorded. In the longitudinal direction along the beam propagation, all electrons are detected with momenta of $p_{e\|} > -1.04$ a.u. since electrons with energies of more than 14.6 eV in the backward direction will overcome the total extraction voltage. After acceleration in the electric field, recoil-ions and electrons traverse drift tubes on either side, each with a length of 22 cm (two times the acceleration distance), in order to obtain a first-order time focus when they reach the two-dimensional position sensitive (2D PS) channel-plate detectors. From the simultaneous measurement of both, position of detection and the time-of-flight (TOF) for each of the particles, in an electron – electron – recoil-ion – projectile coincidence, the recoil-ion charge state and all three momentum components of the recoil-ion and both electrons can be deduced. The two-dimensional position information for a given TOF yields two transverse momenta for each fragment and the TOF provide their longitudinal momentum component. A multi-hit Time to Digital Converter (TDC) permits to record the signals for both electrons if the second electron hits the detector with some time delay with respect to the first one. The minimum time delay needed to identify the two electrons as different particles is ~15 ns. Double ionisation by charged particle impact is completely determined by the measurement of eight out of twelve momentum components. Measuring nine components, as in the present experiment, the missing three momentum components (i.e. the momentum transferred by the projectile) and the Q-value (inelasticity) of the reaction can be deduced from the energy and momentum conservation. An electron momentum resolution of $\Delta p_{e\|} = 0.06$ a.u. in the longitudinal direction and $\Delta p_{e\perp} = 0.14$ a.u. in the transverse direction is achieved. For the

recoil-ions resolutions of $\Delta p_{R\parallel} = 0.13$ a.u. and $\Delta p_{R\perp} = 0.31$ a.u. are obtained in the longitudinal and transverse directions, respectively.

3. Results and discussion

The schematic diagram of the collision geometry considered in the present work is given in figure 1. The scattering plane is defined by the initial projectile direction (z-direction) and the transverse component of the He^{2+} ion (-x coordinate). The azimuthal plane is the plane perpendicular to the collision plane (x-y plane).

In order to simplify the intricate collision dynamics of the four-particle continuum (two electrons, the recoil-ion and the emerging projectile) in a double ionisation event and to identify the gross features of the momentum balance we have successfully tried, as will be shown below, to reduce the four-particle to an effective three-particle continuum by considering the sum momentum of both electrons. This is done easily by adding the two electron momentum vectors for each double ionisation event. In this way, the momentum balance between the recoil-ions, the sum momentum of the electrons and the projectile can be explored and a comparison with single ionisation dynamics becomes possible.

The data have been normalized to the total double ionisation cross section of $\sigma^{2+} = 1.8 \cdot 10^{-15}$ cm^2 which is extrapolated from previous total cross section measurements for the same projectile [Berg 1993] which are accurate within 20%. Due to experimental limitations, electrons with energies only up to ~150 eV were detected with full acceptance and the higher energy electrons (above 150 eV) have reduced acceptance on the detector. From the electron sum-energy distribution it was extrapolated that due to experimental acceptance only 75% of all double ionisation events have been recorded. Thus, the total number of events was normalized to $0.75 \cdot 1.8 \cdot 10^{15}$ cm^2 introducing an additional estimated error of 10 %. In the figures, only statistical error bars are indicated.

3.1 Longitudinal momentum balance

For ionising fast ion-atom collisions without mass transfer, i.e., no electron capture by the projectile, the longitudinal momentum balance is obtained from the momentum and energy conservation relations

$$\Delta p_{p\|} = -(p_{R\|} + \Sigma p_{e\|})$$

$$= -(Q+\Sigma E_e) / v_p$$

where $\Delta p_{p\|}$ is the longitudinal momentum transfer from the projectile, $p_{R\|}$ is the longitudinal recoil-ion momentum, $\Sigma p_{e\|}$ is the longitudinal electron sum momentum; Q is the total inelasticity of the reaction, which is equal to the energy difference between the initial and final atomic states, ΣE_e is the total energy of both ejected electrons and v_p is the initial projectile velocity (for details see Ullrich et al. (1997), Dörner et al. (2000)). This relation is valid for small projectile scattering angles that are well fulfilled for heavy projectile and for large projectile energies where the energy loss in an atomic process is always tiny compared to its initial energy.

The longitudinal momenta of the recoil ion and both of the electrons are shown in figure 2. Due to the measurement, we distinguish the two electrons according to their arrival time on the detector, i.e. their longitudinal momentum, where electron-1 is the first and electron-2 is the second one in each double ionisation event. Both electrons are almost always emitted with opposite longitudinal momenta compared to the He^{2+} ion. Thus, they are preferentially emitted into the forward half sphere, strongly correlated with the He^{2+} recoil-ion and seem to balance its momentum in each single collision.

This is put forward in figure 3, where the longitudinal momentum of the recoil-ion (open circles) is plotted along with the sum-momentum of both electrons (full circles) and the projectile momentum change (histogram). Very obviously, $p_{R\|}$ is nearly completely balanced by the sum-momentum of the two electrons with a quite small net-momentum transfer by the projectile of less than 1 a.u. for the major part of the collisions. $\Delta p_{P\|}$, the longitudinal momentum transfer by the projectile, is deduced (see above equation) from the known Q-value and the measured electron energies. It shows a sharp rise at –0.25 a.u., the minimum longitudinal momentum transfer (Q/v_P) due to the total helium binding energy of 79.0 eV and a tail towards negative momenta resembling the sum-energy spectrum of the two electrons ($\Sigma E_e/v_P$). The deduced projectile momentum distribution is slightly broadened, depending on the electron sum-energy, by about $0.025 \cdot \Sigma E_e$ a.u. (ΣE_e in atomic units) due to the electron energy resolution in the experiment.

Striking similarities to single ionisation dynamics are observed in such a representation considering the electron vector sum-momenta: The “effective electron”, the negatively charged part of the target fragments, is primarily emitted into the forward direction, along the ion-beam propagation, with a peak of the distribution at around 1.7 a.u., whereas the positively charged recoil-ions are ejected backwards with negative momenta peaked at around –1.3 a.u.. As for single ionisation, this forward-backward asymmetry can be understood as a result of the final-state interaction (“post-collision interaction”, PCI) of the target fragments with the emerging highly charged projectile pulling the electrons behind and pushing at the same time the target ion into the backward direction. Since the recoil-ion is doubly charged and the individual electrons are rather slow ($v_e < 4$ a.u.) compared to the swiftly receding ($v_p = 12$ a.u.) projectile, it interacts with a very similar magnitude of force on the negative as well as positive target fragments, resulting in a very similar but oppositely directed momentum distributions.

In other words, the various target fragments can be viewed as being dissociated along the longitudinal direction “after the collision” according to their different charges into two contributions. Whereas the actual collision time τ, where ionisation takes place, can be estimated to be rather short $\tau \sim 1/\Delta E$, a fraction of an atomic unit for a given energy transfer of $\Delta E \sim \Sigma E_e > 1$ a.u., the “dissociation” time is quite large: even 10 a.u. in time after the collision occurred, the potential energy between the projectile and the target-fragment charge clouds is about one atomic unit, justifying the “post” collision interaction picture. Thus, it seems to be quite plausible to consider negatively and positively charged parts of the target fragments as single effective particles, each moving along the longitudinal direction. The same is much less obvious in the transverse direction and will be explored in the following section.

3.2 Transverse momentum balance

As for the longitudinal direction, the direct measurement of the projectile momentum transfer by detecting the projectile scattering angle is practically impossible due to its small magnitude of typically less than μradian. But, again it can be deduced from the measured quantities, in this case from the transverse momenta of the recoil-ion and both electrons with a resolution of 0.34 a.u. using the momentum balance equation

$$\Delta \mathbf{p}_{p\perp} = -(\mathbf{p}_{R\perp} + \Sigma \mathbf{p}_{e\perp})$$

where $\mathbf{p}_{R\perp} = (p_{Rx}, p_{Ry})$ and $\Sigma\mathbf{p}_{e\perp}$ are the transverse recoil-ion and electron sum momentum vectors, respectively. The transverse momentum exchange is directly coupled to the projectile scattering angle θ_P by the relation

$$|\Delta p_{p\perp}| = \theta_P M_p v_p$$

where M_p is the projectile mass and v_p is the velocity of the incident ion beam.

In order to explore whether or not the "effective" three-particle picture also holds along the transverse direction, we start by inspecting the single differential cross sections as a function of the transverse momenta of the recoil ion, both electrons and the projectile, which are shown in figure 4. Similar as in the longitudinal direction, the main momentum balance indeed occurs between the recoiling target ion and both emerging electrons with nearly identical momentum distributions up to $p_\perp \leq 5$ a.u., resulting in a relatively small transverse momentum change of the projectile, or scattering angles of less than 1 μradian. Thus, even in the transverse direction, the complicated four-body dynamics seems to essentially reduce to an effective three-body continuum. Such a feature strongly suggests that these "two" collision fragments, the recoil-ion and the electron centre-of-mass are emerging back-to-back with similar and opposite momenta. It is also seen that the slope of the projectile momentum distribution is less steep and merges with that of the electron sum and recoil-ion at around $p_\perp \approx$ 2.5 a.u..

In order to explore the transverse momentum balances in more detail, we have plotted the transverse momentum of recoil-ion versus the sum momentum of both electrons in a two-dimensional plot (see figure 5). The cluster size corresponds to the doubly differential cross section $d^2\sigma/(dp_{\Sigma e\perp}\, dp_{R\perp})$ on a logarithmic scale. The cross section is peaked along the diagonal line where the transverse momentum of the recoil-ion is equal to that of the sum momentum of the two electrons (i.e, $|\mathbf{p}_{R\perp}| = |\Sigma\mathbf{p}_{e\perp}|$). In more than 75 % of all events they balance their momenta within ± 1.0 a.u.

In figure 6 the correlated transverse emission between the recoil ion and both electrons is explored in analogy to figure 2. Here, a transverse axis is defined by the projection of the recoil-ion momentum vector onto the azimuthal (x-y) plane (see figure 1), projecting then the momentum vectors of both electrons onto this axis. Note that in this coordinate system the x-component of the recoil-ion is by definition always negative. Strikingly, and nearly as

pronounced as in the longitudinal direction, both electrons are found to be strongly correlated with the He^{2+} ion emerging nearly exclusively into opposite half spheres. Moreover, electron "one" and "two", numbered according to their relative longitudinal momenta ($p_{e1\|} > p_{e2\|}$), display nearly identical momentum distributions. This implies, that transverse and longitudinal momentum balances are largely independent from each other. Further, a pronounced maximum at near zero transverse momentum is observed as a result of the He^{2+} Coulomb potential singularity, giving rise to a "cusp-shaped" electron emission pattern even in the transverse direction. Due to the unique numbering of the electrons with respect to their relative velocity in the longitudinal direction, this feature is only observed for electron "two" (see also in fig.2).

To further elucidate the effective three-particle nature of the four-particle dynamics, we present the full transverse momentum balance between the recoil-ion, the electron center-of-mass and the projectile momentum in figure 7 in a similar plot as for the longitudinal direction in figure 3. While the momentum transfer by the projectile plays a more important role in the transverse momentum balance as compared to the longitudinal direction (figure 3), still the major characteristic, namely the predominant balance of $\mathbf{p}_{R\perp}$ by the electron transverse momentum sum, prevails.

This might seem to be quite surprising at first glance, since in the present regime of large perturbation ($q/v_P = 4.4$), it is very well established that double ionisation is dominated by a "two-step interaction" (TS-2, McGuire et al (1995)), where the projectile interacts with both of the electrons independently, transferring independently energy and momentum to each of them. Consequently, we might expect that the projectile knocks out both electrons in two "subsequent binary-like" collisions, thus, compensating the electrons sum-momentum and leaving the target nucleus merely as a spectator, which definitely is in contrast to the experimental observation. Instead, the projectile transverse momentum transfer is considerably less than the momenta of the fragments. This implies that the highly-charged projectile does not predominantly interact in binary-like collisions independently with both of the target electrons but rather seems to dissociate the target even in the transverse direction by interacting simultaneously with a similar force but opposite direction onto both electrons and the nucleus at "large" impact parameters. Thus, again mainly energy is transferred to the target to eject the electrons in a dipole- (or photon-) like interaction with quite small net-momentum transfer to the whole target system. In the limit of vanishing momentum transfer double ionisation is reduced to a three particle, and, by considering the electron centre-of-mass motion only, it is

even further reduced to an effective two-particle system. Double ionisation under these conditions has been discussed within the Weizsäcker–Williams equivalent photon method as a simultaneous absorption of several virtual photons from the field [Moshammer et al. (1996); Keller et al. (1997)], but this is certainly not rigorously applicable for the slow collisions considered in the present experiment. For a detailed analysis of the limitation of this method, its connection to the Bethe-Born limit and to ionisation by real photons, see the recent publication by Voitkiv and Ullrich (2001).

3.3 Complete momentum balance in the collision plane

In order to summarise the previous sections and visualise the momentum balance in both dimensions (transverse and longitudinal) simultaneously, we use a plane defined by the incident projectile momentum and the outgoing transverse momentum of the He^{2+} ion (collision plane). Projections of the momentum vectors onto the collision plane are presented in figure 8 for all reaction products, again only considering the sum momenta of both electrons.

Two prominent features that have been discussed and observed already in the previous sections are noticed again in the figure. First, even in two dimensions, the electron sum and the recoil-ion momenta are oriented in very good approximation into opposite directions. Also in magnitude, the recoil-ion mainly compensates the sum momenta of both electrons, as can be seen from the relatively small momentum change of the projectile. In this representation it is quite obvious, that the momentum balance is significantly less perfect in the transverse direction. Second, again a forward-backward asymmetry is clearly seen, as a direct consequence of the post collision interaction caused by the long-range potential of the receding Au^{53+} projectile. The shift of the momentum distribution from $p_{\|} = 0$ and the asymmetry of the distribution for the present case reveal the actual strength of the PCI. As the perturbation or the collision time decreases, the shift decreases as well and moves towards $p_{\|} = 0$. Simultaneously, the distribution becomes more symmetric as has been observed for single ionisation by 1 GeV/u U^{92+} [Moshammer et al (1997)] and 100 MeV/u C^{6+} impact on helium [unpublished].

Similar features have recently been noticed even for triple ionisation by Schulz et al. (2000). In fact, considering the centre-of-mass motion of the ejected electrons in double or even triple ionisation of He or Ne by fast highly-charged projectiles at large perturbations,

essentially all characteristic dynamic features observed for single ionisation [Moshammer et al. (1997)] are rediscovered.

3.4 Momentum balance in the azimuthal plane

To further elucidate and explore the fragment's correlated dynamics in the scenario of an effective three-particle break-up reaction, we projected the momentum vectors of all three-particle momenta onto the azimuthal plane, i.e. the plane perpendicular to the incoming projectile (x-y plane).

In figure 9, the azimuthal emission direction (not the magnitude of its momentum) of either one of the emitted particles is fixed along the indicated arrow and the momentum distribution of the others (direction and magnitude) is visualised in a two-dimensional representation. The projected electron sum-momenta distribution with respect to the recoil-ion emission direction is presented in figure 9a. The electron sum-momentum distribution is clearly peaked towards the positive side of p_x with its maximum opposite to that of the recoil-ion direction. Exact 180° scattering of "both" fragments would correspond to the photoionisation situation, which is clearly not realised at all in the present situation. Inspection of the projectile distribution with respect to the recoil-ion emission direction shows a significantly weaker correlation (figure 9b). It is slightly more pronounced for larger transverse projectile deflections, where projectiles and recoil-ions, i.e. both nuclei start to predominantly exchange momenta in presumably closer collisions at smaller impact parameters. Finally, in the projection of the electron sum-momenta with respect to the projectile an even weaker correlation, hardly recognized at all, is observed (figure 9c). Electrons are distributed almost isotropically around the centre signifying again very clearly the complete absence of two-body binary-like encounters of the projectile with each of the two electrons to result in double ionisation.

The correlated angular emission can be further illustrated when polar plots are used on the expense of loosing the momentum information in figure 10. It is very transparent from the polar plots that among the "three" different "two-body" correlations of the effective three-particle continuum the one between the recoil-ion and electrons centre-of-mass are the strongest, underlining again the dominance of dipole like transitions in double ionisation of helium at strong perturbations. In addition, some reminiscence, mainly at larger transverse

momentum transfer, of the inter-nuclear repulsion is observed where the target nucleus in average tends to go with little preference into the direction opposite to the projectile deflection. Finally, the electron sum-momentum angular distribution is quite isotropic with respect to the projectile transverse momentum transfer in the azimuthal direction again with a slight preference to the opposite direction. Among other features, the latter both indicate deviations from an ideal “dissociation” of the target in the projectile field.

Conclusions

We have performed a kinematically complete experiment on double ionisation of helium by fast highly-charged ion impact using a reaction microscope to detect the momentum vectors of all emerging fragments, largely independent of their relative emission direction and energy. From the investigation of momentum balances between collision fragments, a striking similarity is observed between single and double ionisation if the centre-of-mass motion of the two electrons is considered instead of their individual momenta. Similar to single ionisation dynamics, a pronounced forward-backward asymmetry has been observed in the longitudinal momentum distributions of the electrons sum and the recoil ions, which is explained in terms of the PCI. Also, in the transverse direction, the correlation of the electrons sum with the recoil-ion is clearly more pronounced than their correlation with the projectile.

However, especially the latter feature, on first sight seems to contradict the well-acknowledged dominance of TS-2 to contribute to double ionisation in the present regime of large perturbations, where the projectile collides independently with both of the target electrons exchanging independently energy and momentum with them and, thus, finally is expected to compensate the electrons sum-momentum. It is suggested, however, that the present results do not really contradict the dominance of TS-2 but strongly support a special realisation of this undoubtedly dominant contribution for most of the double ionisation events in the present collision system. Thus, a picture might be brought forward, that the fast highly-charged projectile passes the target at large impact parameters well outside the electronic shell radius of the helium atom. Then, a similar but oppositely directed momentum is transferred to the negative electron cloud $\mathbf{p}_{\Sigma e}$ and to the positively charged target nucleus $\mathbf{p}_R$ resulting in a relatively small net-momentum transfer $\mathbf{q} = \mathbf{p}_R + \mathbf{p}_{\Sigma e} = -\Delta\mathbf{p}_P \sim 0$ to the target as a whole and, consequently, in a small projectile deflection. The target, thus, might be seen as effectively being “ripped apart”, dissociated in the strong projectile field. In the perturbation-expansion

language this would correspond to a TS-2 mechanism, however, to a quite special realisation, where the momentum transfer to both target electrons and to the nucleus are not independent in each single collision but indeed are very similar in magnitude but in opposite direction. This, together with the fact, that the momentum transferred to each individual electron is almost identical $\mathbf{q}_{e1} \sim \mathbf{q}_{e2}$, describing a scenario, where both electrons are effectively displaced from their nucleus during a short time interval – the collision time – as compared to their classical orbiting time in the atom. Then, in a sense, we are approaching a situation, where the nuclear potential is "suddenly" switched off, a scenario suggested by Heisenberg (1947) and recently picked up for neutron on helium collisions (Berakdar (2001)), which might be considered to be an ideal situation to investigate the short-time correlation of bound-state electrons.

We gratefully acknowledge support from GSI, the Leibniz-Programm of the Deutsche Forschungsgemeinschaft from the BMBF, the Max-Planck-Institut für Kernphysik and the National Science Foundation.

References

Bapat B, Keller S, Moshammer R, Mann R and Ullrich J, J. Phys. B: At. Mol. Opt. Phys. **33** (2000) 1437

Bapat B, Moshammer R, Keller S, Schmitt W, Cassimi A, Adoui L, Kollmus H, Dörner R, Weber Th, Khayyat K, Mann R, Grandin J P and J. Ullrich, J. Phys. B: At. Mol. Opt. Phys. **32** (1999) 1859

Berakdar J (submitted to J. Phys. B) and private communication

Berg H B, Ph.D. Thesis, (1993) Universität Frankfurt

Briggs S and Schmidt V, J. Phys. B: At. Mol. Opt. Phys. **33** (2000) R1

Bronk T, Reading F H and Ford A L, J. Phys. B: At. Mol. Opt. Phys. **31** (1998) 2477

Dorn A, Kheifets A, Schröter C D, Najjari B, Höhr C, Moshammer R and Ullrich J, Phys. Rev. Lett. **86** (2001) 3755

Dorn A, Moshammer R, Schröter C D, Zouros T J M, Schmitt W, Kollmus H, Mann R and Ullrich J, Phys. Rev. Lett. **82** (1999) 2496

Dörner R, Bräuning H, Feagin J M, Mergel V, Jagutzki O, Spielberger L, Vogt T, Khemliche H, Prior M H, Ullrich J, Cocke C L and Schmidt-Böcking H, Phys. Rev. A **57** (1998) 1074

Dörner R, Feagin J M, Cocke C L, Braeuning H, Jagutzki O, Jung M, Kanter E P, Khemliche H, Kravis S, Mergel V, Prior M H, Schmidt-Böcking H, Spielberger L, Ullrich J, Unverzagt M and Vogt T, Phys. Rev. Lett. **77** (1996) 1024

Dörner R, Mergel V, Jagutzki O, Spielberger L, Ullrich J, Moshammer R and Schmidt-Böcking H, Phys. Rep. **330** (2000) 95

Fainstain P D, Gulyas L and Dubois A, J. Phys. B: At. Mol. Opt. Phys. **31** (1998) L171

Giese J P and Horsdal E, Phys. Rev. Lett. **60** (1988) 2018

Heisenberg , Z. Phys. **43** (1927) 172

Huetz A and Mazeau, Phys. Rev. Lett. **85** (2000) 530

Keller S, Lüdde H J and Dreizler R M, Phys. Rev. A **55** (1997) 4215

Kirchner T, Gulyas L, Schulz M, Moshammer R and Ullrich J (submitted to Phys. Rev. A)

Lahmam-Bennani A, Duguet A, Gaboriand M N, Taouil I, Lecas M, Kheifets A S, Berakdar J and Dal Cappello C, J. Phys. B: At. Mol. Opt. Phys. **34** (2001) 3073

Lahmam-Bennani A, Taouil I, Duguet A, Lecas M, Avaldi L and Berakdar J, Phys. Rev. A **59** (1999) 3548

McGuire J H, Berrah N, Bartlett R J, Samson J A R, Tanis J A, Cocke C L and Schlachter A S, J. Phys. B: At. Mol. Opt. Phys. **28** (1995) 913

Mergel V, Dörner R, Khayyat Kh, Achler M, Weber T, Jagutzki O, Lüdde H J, Cocke C L, and Schmidt-Böcking H, Phys. Rev. Lett. **86** (2001) 2257

Moshammer R, Schmitt W, Ullrich J, Kollmus H, Cassimi A, Dörner R, Jagutzki O, Mann R, Olson R E, Prinz H T, Schmidt-Böcking H, and Spielberger L, Phys. Rev. Lett. **79** (1997) 3621

Moshammer R, Ullrich J, Kollmus H, Schmitt W, Unverzagt M, Jagutzki O, Mergel V, Schmidt-Böcking H, Mann R, Woods C J and Olson R E, Phys. Rev. Lett. **77** (1996) 1242

Moshammer R, Ullrich J, Kollmus H, Schmitt W, Unverzagt M, Schmidt-Böcking H, Wood C J and Olson R E, Phys. Rev. A **56** (1997) 1351

Reddish T J, Wightman J P, MacDonald M A and Cvejanovic, Phys. Rev. Lett. **79** (1997) 2438

Rescigno T N, Baertschy M, Isaacs W A and McCurdy C W, Science **286** (1999) 2474

Schulz M, Moshammer R, Schmitt W, Kollmus H, Feuerstein B, Mann R, Hagmann S and Ullrich J, Phys. Rev. Lett. **84** (2000) 863

Schulz M, Moshammer R, Schmitt W, Kollmus H, Mann R, Hagmann S, Olson R E and Ullrich J, Phys. Rev. A **61** (2000) 022703

Schwarzkopf O, Krässig B, Elminger J and Schmitt V, Phys. Rev. Lett. **70** (1993) 3008

Taouil T, Lahmam-Bennani A, Duguet A and Avaldi L, Phys. Rev. Lett. **63** (1998) 4600

Ullrich J, Moshammer R, Dörner R, Jagutzki O, Mergel V, Schmidt-Böcking and Spielberger L, J. Phys. B: At. Mol. Opt. Phys. **30** (1997) 2917

Voitkiv A and Ullrich J, J. Phys. B: At. Mol. Opt. Phys. **34** (2001) 4513

Wood C J, Olson R E, Schmitt W, Moshammer R and Ullrich J, Phys. Rev A **56** (1997) 3746

Figure Captions

Figure 1

Schematic diagram of the collision geometry.

Figure 2

Longitudinal momentum distributions for recoil ions and both of the ejected electrons for double ionisation of helium by 3.6 MeV/u Au^{53+} collisions.

Figure 3

Longitudinal momentum distributions for recoil ions and the sum of both electrons along with the projectile momentum loss for 3.6 MeV/u Au^{53+} on He collisions. The full histogram indicates the projectile momentum loss obtained from the known Q-value and the measured electron energies.

Figure 4

The cross section differential in transverse momenta of recoil ions, electrons and the projectile momentum exchange for double ionisation of He by 3.6 MeV/u Au^{53+} impact.

Figure 5

The double differential cross section $d^2\sigma/(dp_{\Sigma e\perp}\, dp_{R\perp})$ for the same collision system in a two-dimensional representation. The z-axis is on a logarithmic scale representing the cross section between $4.0 \cdot 10^{-17}$ cm^2 $a.u.^{-2}$ and $3.0 \cdot 10^{-15}$ cm^2 $a.u.^{-2}$ with 10 steps.

Figure 6

Transverse emission distributions of the recoil ions and both of the ejected electrons. The transverse axis is defined by the projection of the recoil ion momentum vector onto the azimuthal plane (x-y).

Figure 7

Transverse emission distributions of the recoil ion and the sum-momentum of the electrons along with the projectile momentum, the geometry is same as figure 6.

Figure 8

Projections in momentum space of all particles in the final state after helium double ionisation onto the plane determined by the incoming projectile velocity vector and the scattered recoil ion momentum vector (collision plane). The cluster size corresponds to the doubly differential cross section $d^2\sigma/(dp_x\ dp_{//})$ on a logarithmic scale varying between $1.0\cdot\ 10^{-17}$ cm^2 $a.u.^{-2}$ and $1.0\cdot\ 10^{-15}$ cm^2 $a.u.^{-2}$ with 10 steps. For the recoil ion this is equivalent to $d^2\sigma/(dp_{R\perp}\ dp_{//})$ since the recoil ion momentum component vector pointing out of the paper plane is zero due to the specific projection.

Figure 9

The double differential cross sections $d^2\sigma/(dp_x\ dp_y)$ are presented on a logarithmic scale. The z-axis varies between $9.0\cdot\ 10^{-18}$ cm^2 $a.u.^{-2}$ and $7.0\cdot\ 10^{-16}$ cm^2 $a.u.^{-2}$ in 10 steps. The momenta of the a) projectile and b) electrons are projected onto the azimuthal plane, i.e., the plane perpendicular to the projectile velocity vector c) Electron momentum distribution projected onto the azimuthal plane with respect to the projectile.

Figure 10

Singly differential cross section as a function of azimuthal angle $d\sigma/d\varphi$ between the collision fragments transverse momentum vectors.

Fig.1

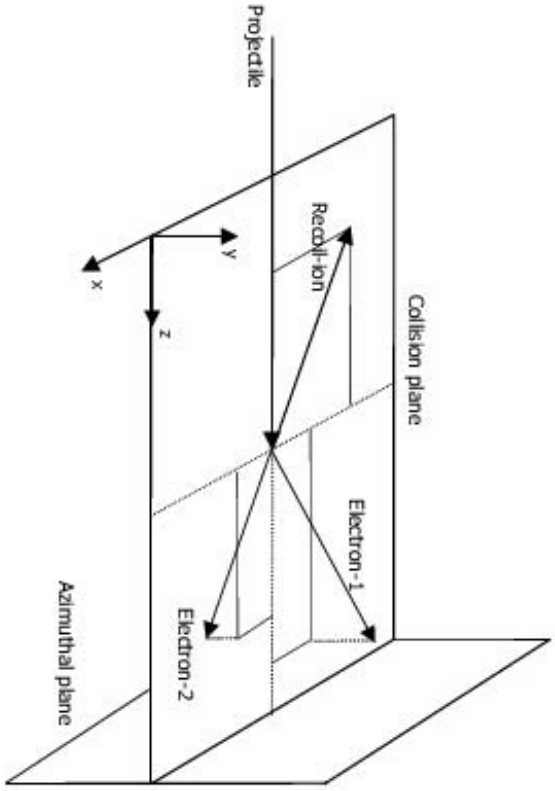
Projectile
Recoil-ion
Collision plane
y
x
z
Electron-1
Electron-2
Azimuthal plane

Fig.2

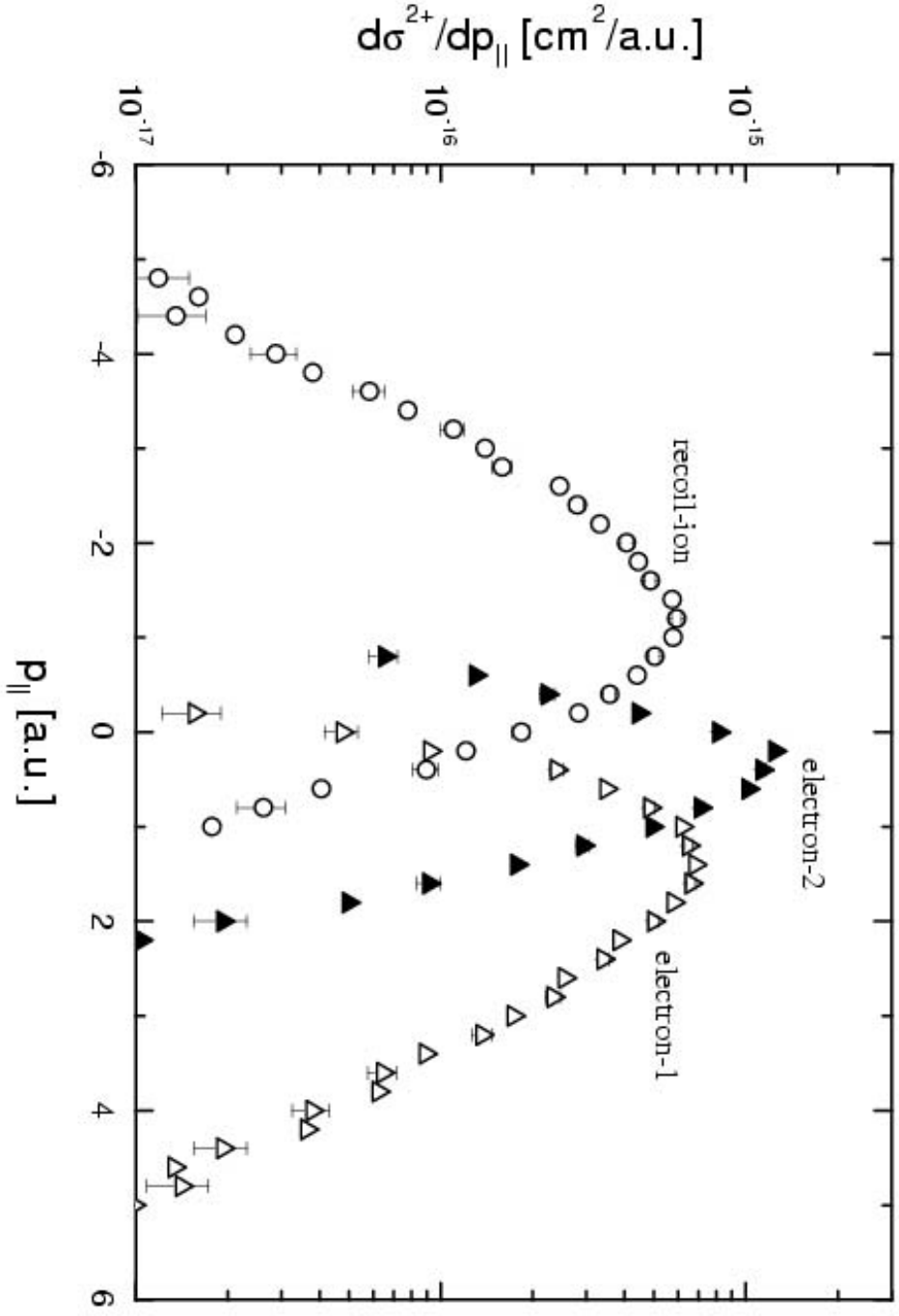
dσ2+/dp|| [cm2/a.u.]
10-15
10-16
10-17
recoil-ion
electron-2
electron-1
p|| [a.u.]
-6
-4
-2
0
2
4
6

Fig.3

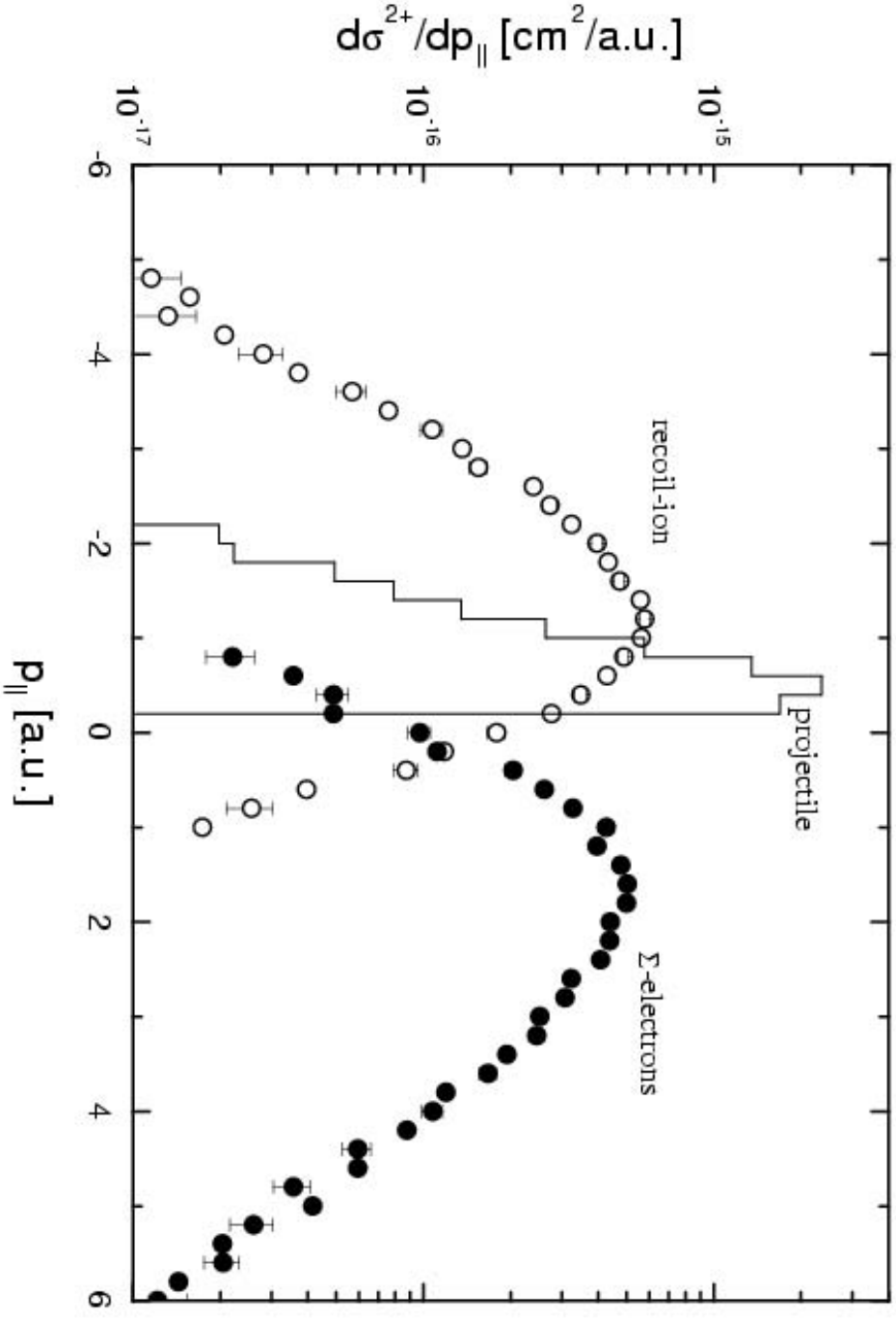
dσ2+/dp|| [cm2/a.u.]
10-15
10-16
10-17
-6
-4
-2
0
2
4
6
p|| [a.u.]
recoil-ion
projectile
Σ-electrons

Fig.4

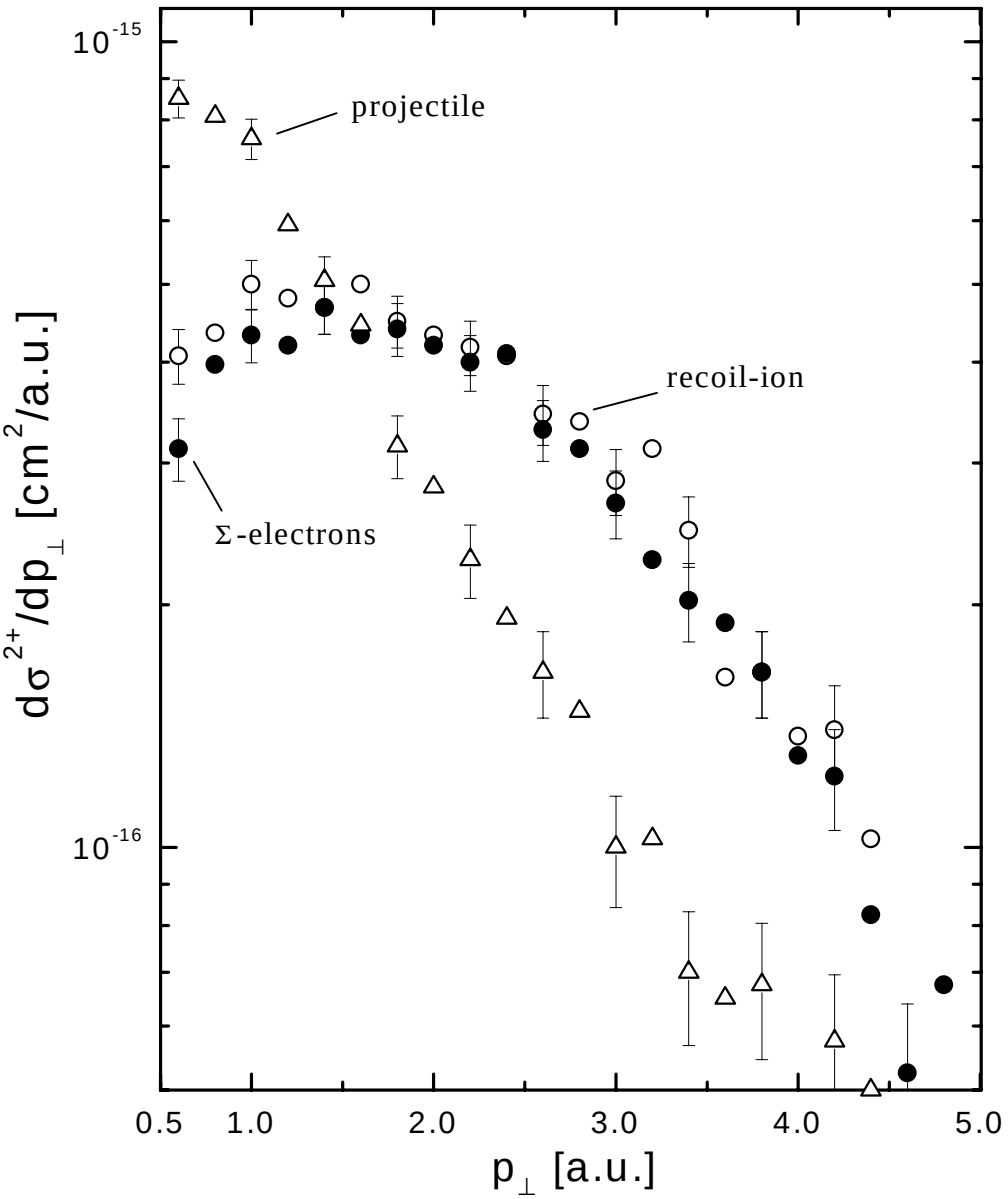
10^-15
10^-16
projectile
recoil-ion
Σ-electrons
dσ^2+/dp⊥ [cm^2/a.u.]
0.5
1.0
2.0
3.0
4.0
5.0
p⊥ [a.u.]

Fig.5

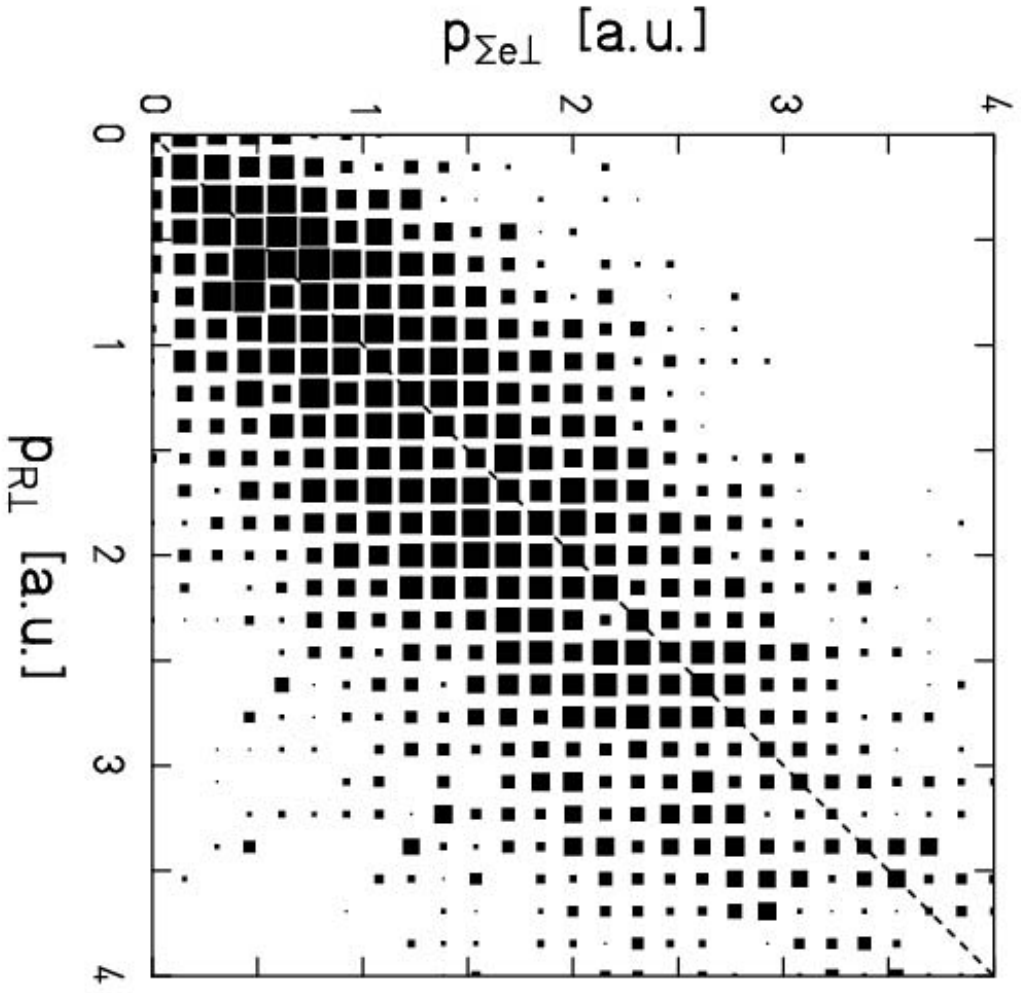

Fig.6

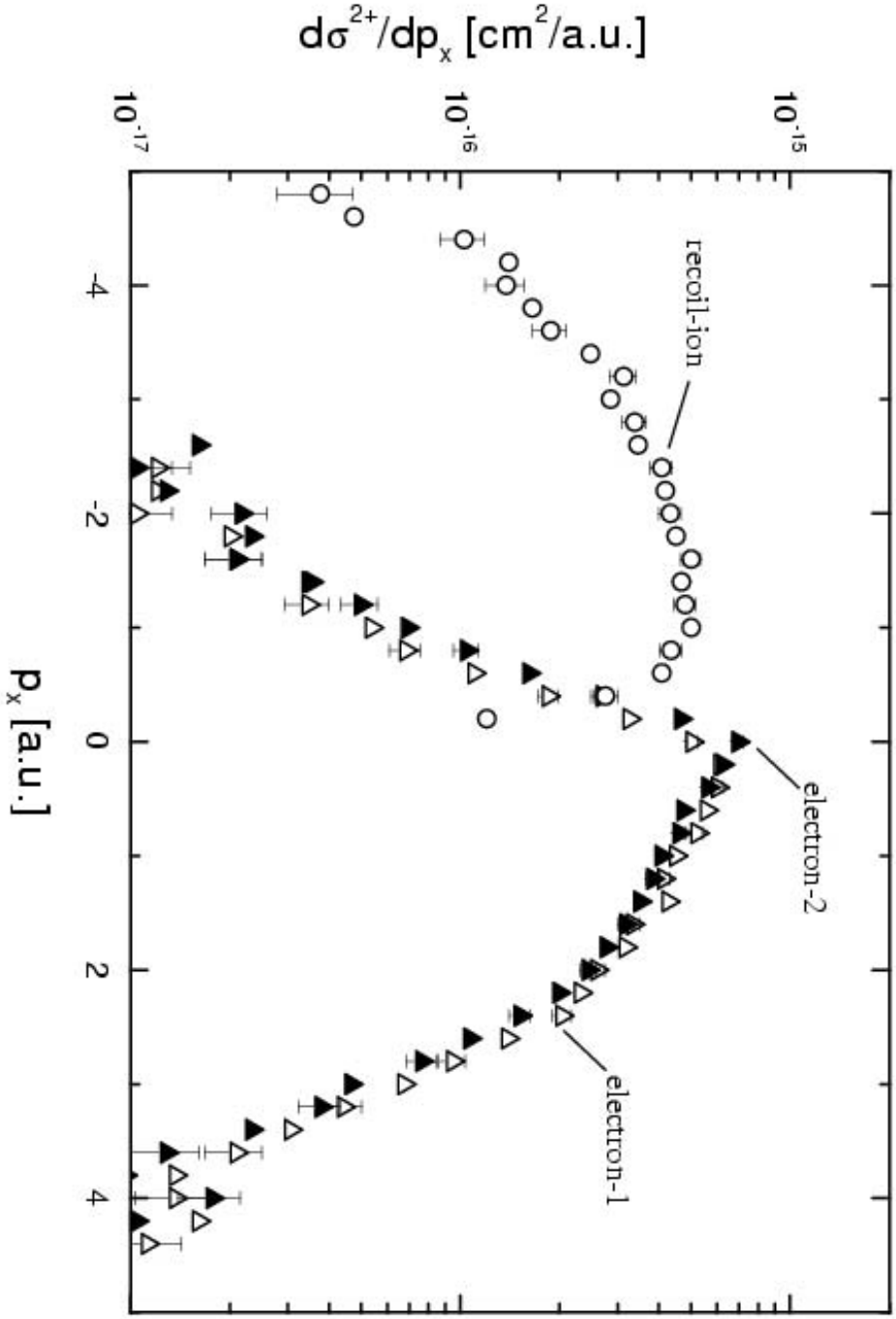
dσ2+/dpx [cm2/a.u.]
10-15
10-16
10-17
recoil-ion
electron-2
electron-1
-4
-2
0
2
4
px [a.u.]

Fig.7

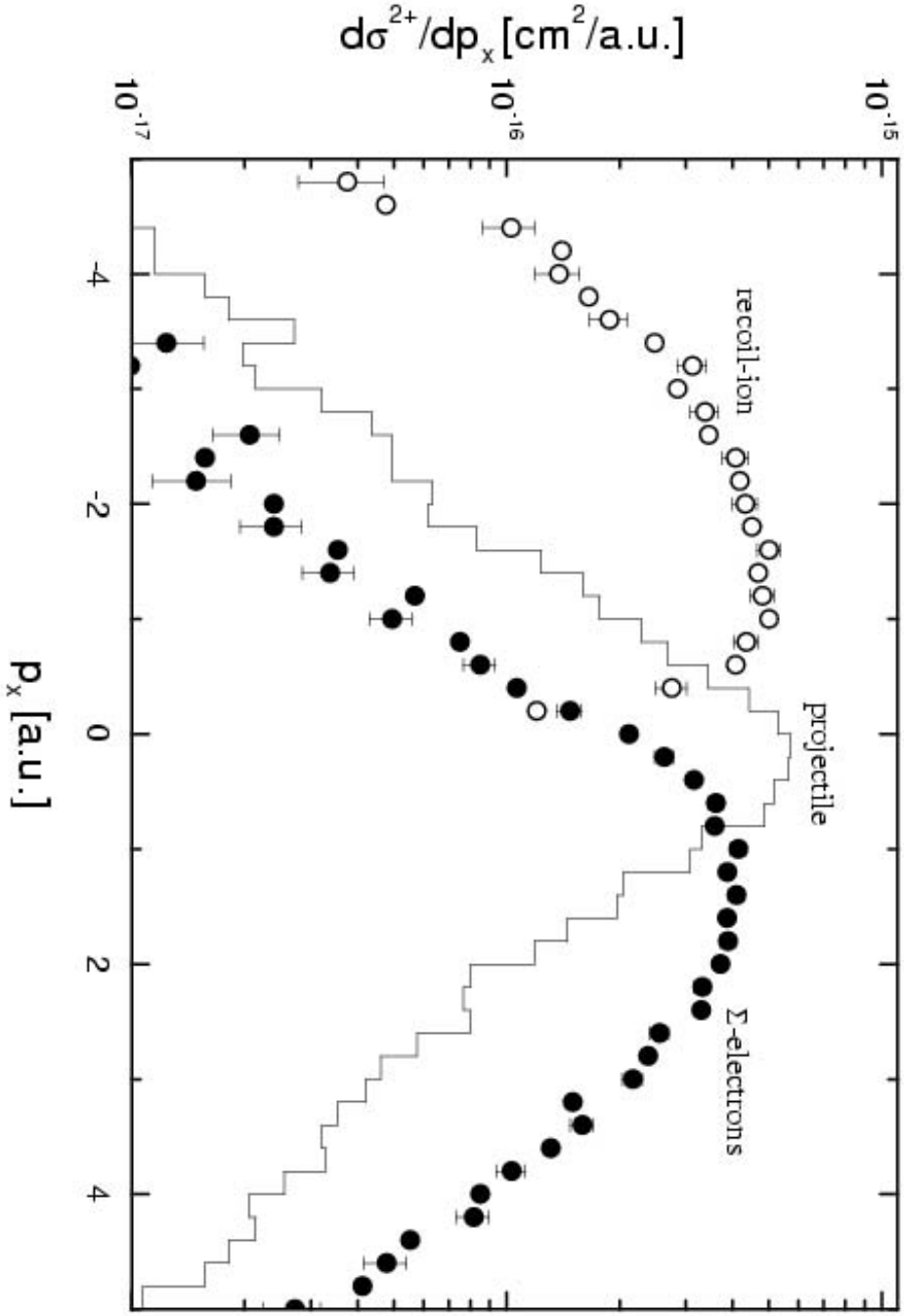
dσ2+/dpx [cm2/a.u.]
10-15
10-16
10-17
recoil-ion
projectile
Σ-electrons
-4
-2
0
2
4
px [a.u.]

Fig.8

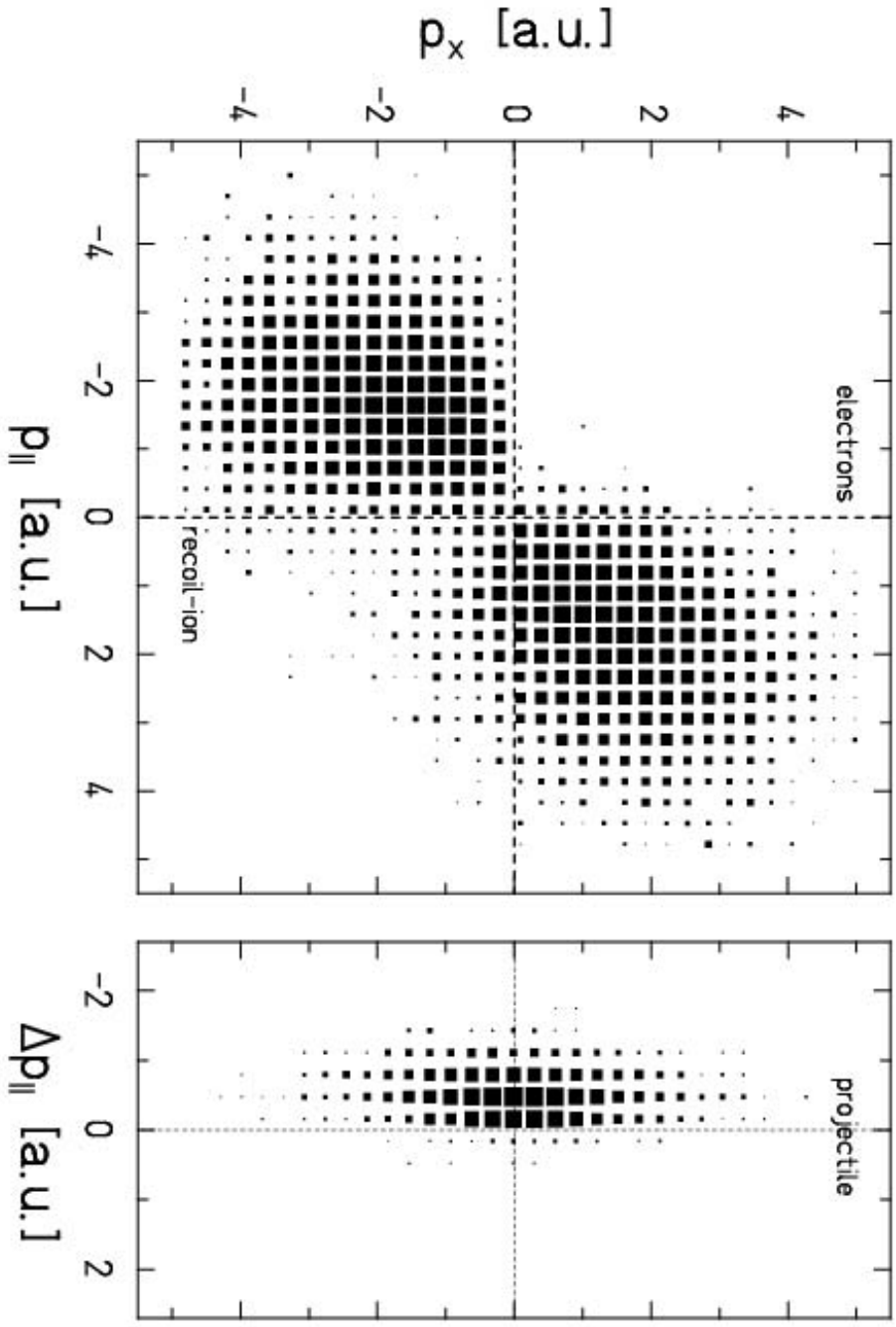
p_x [a.u.]
-4
-2
0
2
4
p_∥ [a.u.]
-4
-2
0
2
4
electrons
recoil-ion
Δp_∥ [a.u.]
-2
0
2
projectile

Fig.9

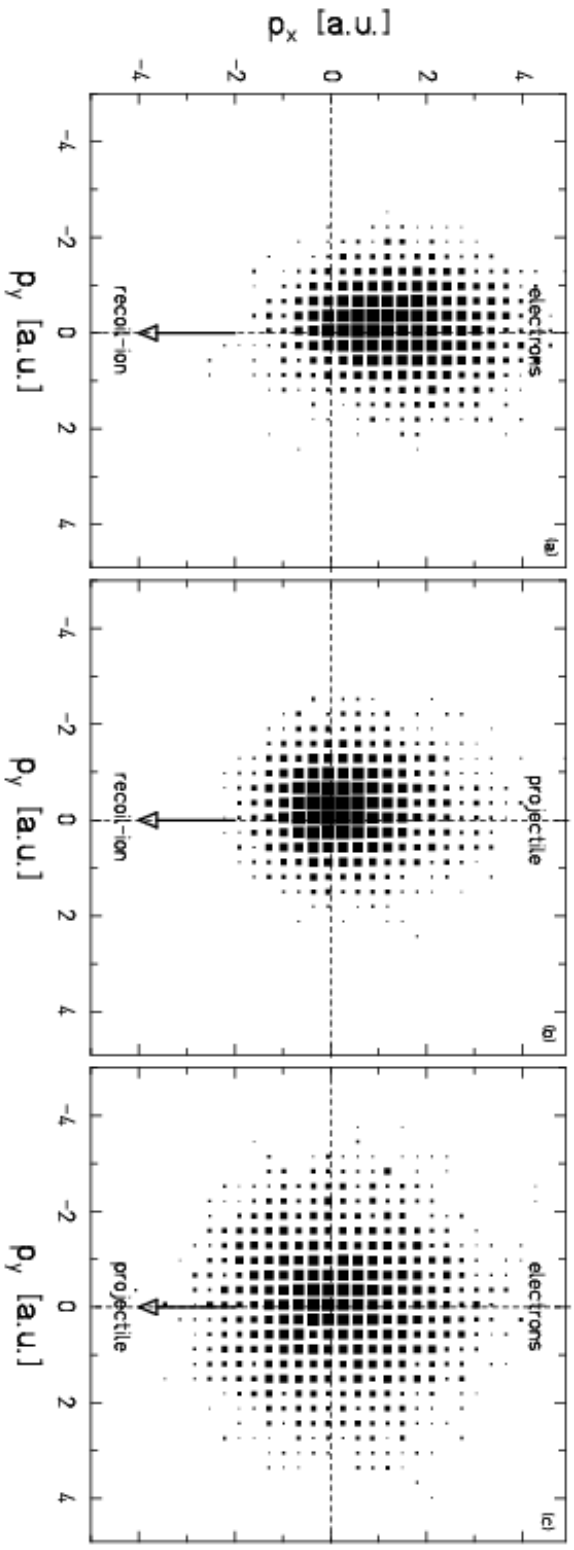
p_x [a.u.]
p_y [a.u.]
electrons
recoil-ion
(a)
projectile
recoil-ion
(b)
electrons
projectile
(c)

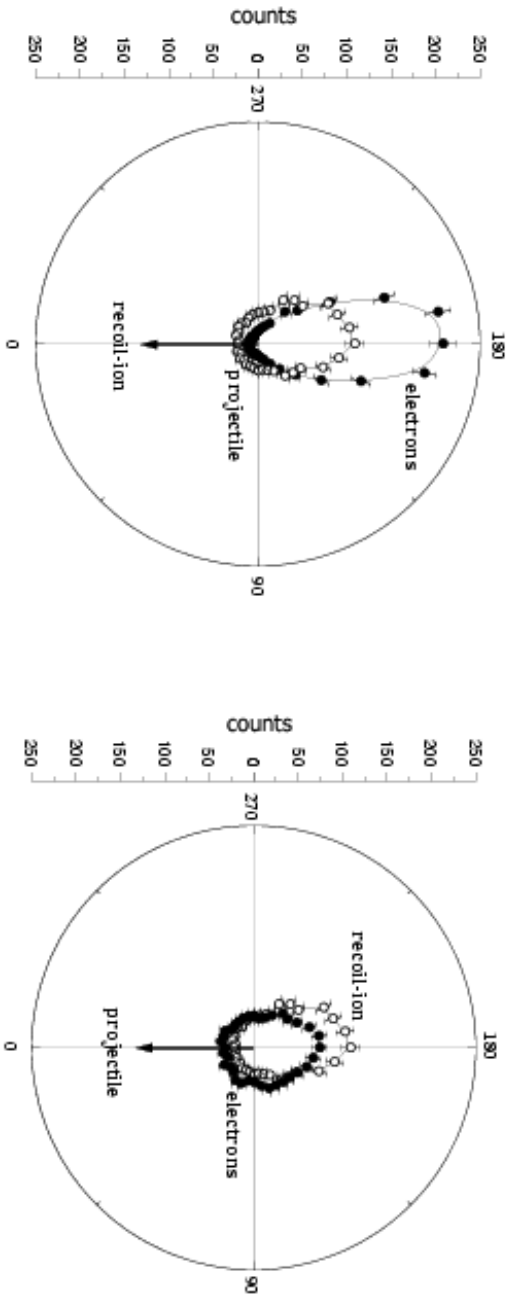
counts
0
50
100
150
200
250
270
0
180
90
recoil-ion
projectile
electrons
counts
0
50
100
150
200
250
270
0
180
90
recoil-ion
projectile
electrons